mmWave Channel Sounding for Vehicular Communications

Nicholas Attwood, François Gallée, Patrice Pajusco, Marion Berbineau

mmWave Channel Sounding for Vehicular Communications

Nicholas ATTWOOD*, François GALLEE*, Patrice PAJUSCO*, Marion BERBINEAU †
*IMT-Atlantique - Lab-STICC, Brest, France, [nicholas.attwood, francois.gallee, patrice.pajusco]@imt-atlantique.fr
†Université Gustave Eiffel, COSYS-LEOST, Lille, France, marion.berbineau@univ-eiffel.fr

***Abstract*—This paper provides initial findings from a Vehicle-to-Infrastructure radio channel measurement campaign. The channel sounder used is the IMT Atlantique SIMO (Single Input Multiple Output) SDR (Software Defined Radio), operating at a frequency of 60 GHz with a bandwidth of 180 MHz. The transmitter (Tx) is mounted on the roof of a moving car, and the receiver (Rx) is positioned like a traffic sign . The measurement scenario is a street with vehicles parked on both sides of the road. For each scenario, the paper presents measurements of the Channel Transfer Function (CTF) gain, the Power Delay Profile (PDP), and the Doppler spread average function.**

***Index Terms*—channel sounder, mmWave, antennas, propagation, measurements, V2X, Vehicle-to-Infrastructure.**

I. Introduction

Channel characterization and modeling are very active research fields, especially in the millimeter-wave (mmWave) domain, owing to the advancements in the 5G NR and beyond standards. Furthermore, within the automotive domain, Vehicular-to-Everything (V2X) communications have emerged as a critical topic over the last decade. The utilization of the 60 GHz frequency band stands out due to its ability to provide significantly wider bandwidths compared to lower frequencies. Various recent works deal with radio channel characterization in the mmW band for vehicular applications considering different channel sounders.

The initial device discussed is a sounder that utilizes a pseudo-random sequence developed by Ilmenau. This sounder, known as DP-UMCS (Dual Polarized Ultra-wideband Multi-Channel Sounder), boasts a bandwidth of 6.75 GHz in the mmW band, allowing for measurements in cross-polarization. In [1], the focus is on studying the impact of a "T"-shaped intersection in vehicle-to-vehicle communication. Static measurements enable an azimuthal analysis of various scatterers in the scene, complemented by a power analysis to distinctly identify different scatterers.

Moving on to [2], the same sounder is employed to investigate the effect of a vehicle obstructing communication between the transmitter and receiver. The University of Brno has developed a sounder utilizing PN (Pseudo-Noise) sequences with an 8 GHz bandwidth, applied for both static and dynamic measurements. [3] involves a dynamic measurement scenario, illustrating a car passing in front of a university building, with an environment featuring trees and parked vehicles along the path.

In [4], an analysis of the link between two vehicles is conducted, involving a crossing at a speed of approximately 50 km/h. The University of Vienna introduces a flat-spectrum sounder in the mmW band with a 500 MHz bandwidth in [5]. The authors investigate the effect of one vehicle overtaking another, with a measurement duration of less than 2 seconds and a maximum travel speed of 30 km/h. In [6], the sounder is enhanced to perform Single Input Multiple Output (SIMO) measurements with a longer duration, but still less than 4 seconds.

Addressing the shortage of sounders capable of dynamic SIMO measurements in the mmW band within a minute while remaining non-restrictive, IMT Atlantique/Lab-STICC has developed a channel sounder with the ability to conduct dynamic measurements, saving several minutes of data, and offering a bandwidth of 180 MHz. The subsequent sections of the paper are organized as follows: Section II presents the specifications of this channel sounder, Section III describes the measurements, and Section IV highlights the results. The last section is devoted to future works and conclusion.

II. The IMT-A's SIMO Channel Sounder at 60 GHz

This section introduces the architecture of the IMT-Atlantique/Lab-STICC's Single Input Multiple Output (SIMO) mmWave channel sounder (CS) designed for measurements in the 60 GHz band developed within the framework of the mmWave4Rail French research project. Figure 1 displays the integrated transmitter (TX) and receiver (RX) components housed within racks for both front-ends. The CS is structured on a Software Defined Radio (SDR) framework, utilizing an Orthogonal Frequency-Division Multiplexing (OFDM) waveform as the excitation signal. To enhance the Power Amplitude to Peak Ratio (PAPR), a Newman phase, as defined in Equation 1, is considered for each multi-tone.

$$\phi_k = \frac{\pi(k-1)^2}{m}, \text{ with } m \text{ the number of multi-tone, and } k \text{ the k-th multi-tone.} \quad (1)$$

The up and down converters on the TX and RX sides are Commercial Off-The-Shelf (COTS) components from Analog Devices, enabling measurements in the V band. The reference of these demonstration boards is EK1HMC6350, enabling us to take measurements up to 200 meters. This measurement distance is limited by the sensitivity of the card at a fixed

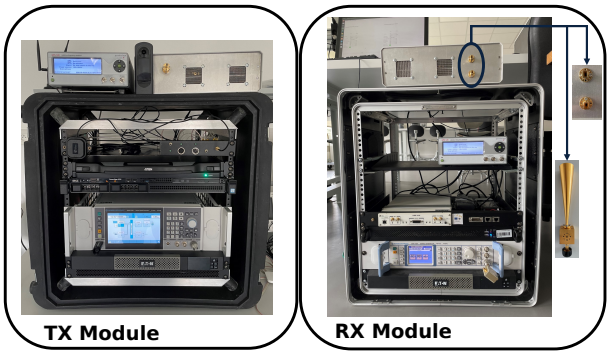

Fig. 1. View of the TX and the RX Module.

TABLE I
MAIN CHARACTERISTICS OF THE CHANNEL SOUNDER

Type	Value
Center Frequency	57 - 60 GHz
Bandwidth	180 MHz
Maximum Excess Delay	2 µs
Rx Antenna	15 dBi horn antenna
Tx Antenna	5 dBi horn antenna
Polarization	Vertical, Horizontal

receiver gain setting. The key specifications of the CS are outlined in Table I and further detailed in [7].

To achieve highly accurate vehicle positioning, the CS is equipped with a Real Time Kinematic Global Navigation Satellite System (RTK GNSS). Furthermore, a 360° camera and a speed sensor are integrated into the CS. The speed sensor serves to anticipate the Doppler shift arising from the relative movement between the TX and RX. Synchronization between the RX and TX components is achieved through two rubidium clocks disciplined by GNSS.

The channel sounder features two antenna configurations. The dual receivers are utilized for Single Input Multiple Output (SIMO) channel measurements, but the antennas can be altered to accommodate a circular horn antenna with an orthomode transducer for cross-polarization measurements. This system offers the advantage of assessing the impact of polarization under identical measurement conditions.

III. MEASUREMENT SCENARIO

The measurement campaign was conducted at the IMT Atlantique Brest Campus. A nearby road, depicted in Fig. 2, was chosen for the measurements. The transmitter was positioned on the car's roof, while the receiver remained fixed at a height of 1.6 meters, approximately matching the height of a typical car or road sign. The road itself spanned a length of 150 meters, featuring parked cars on both sides, as illustrated in Fig. 4. This setup emulates a scenario resembling communication between a car and a traffic sign. The measurement sequence commenced with a Pseudo Non-Line-Of-Sight (PNLOS) situation, leveraging the slight elevation of the road to obstruct the direct Line Of Sight (LOS) to the TX. The parked cars along the road enabled the study of the impact of multiple vehicles on Multi-Path Components (MPCs).

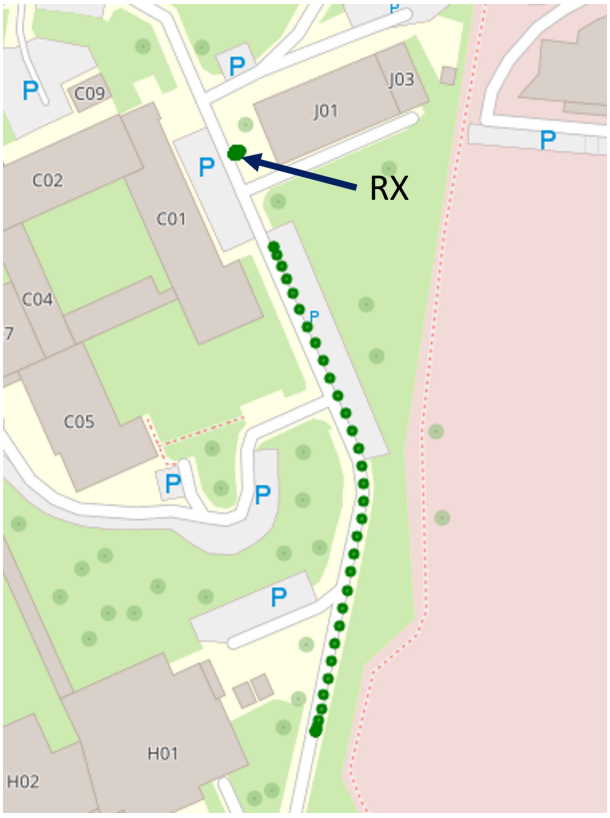

Fig. 2. Localization of the measurement from the GPS RTK.

Fig. 3. View of the TX and the RX Module on the environment.

IV. EXPERIMENTAL RESULTS

A. Pre-Processing of the Data

The configuration of the channel sounder is adjusted to acquire a complex Channel Transfer Function (CTF) at intervals of $\frac{\lambda}{10}$ for a maximum speed of 3 km/h. This setup allows for measurements to be conducted over a duration of 6 minutes. Following the measurements, the CTF is computed using the Inverse Fast Fourier Transform (IFFT) along with a Hanning

Fig. 4. Picture during the measurement from the 360°camera.

window, resulting in a Channel Impulse Response (CIR). The CIR is then averaged using an incoherent moving window with a size of 20λ, moving in steps of 10λ, to derive a Power Delay Profile (PDP) as computed from equation 2.

$$PDP(\tau) = \frac{1}{N}\sum_{i=1}^{N} |h(\tau, t_i)|^2 \tag{2}$$

From the CIR, several parameters can be easily derived, including the maximum excess delay, average delay, Root Mean Square (RMS) delay spread, and the Doppler Spread Function. This function is calculated by extracting each delay until the maximum excess delay surpasses a threshold determined from all CIR measurements. The computation is carried out following equation 3.

$$Doppler_i = TF[h_{iN+(1,\ldots,N)}(\delta_\tau)] \tag{3}$$

where $Doppler_i$ is the i^{th} delay Doppler and δ_τ is all index that correspond to LOS or MPCs.

B. Large Scale Fading

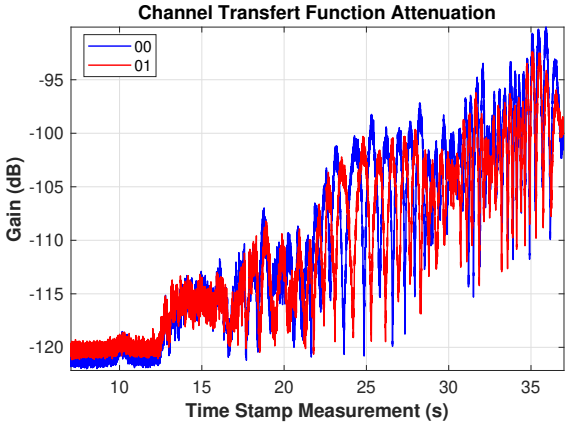

Fig. 5. The gain of the CTF during the measurement. In blue, for the first channel from the antenna on top of the front-end and in red for the second channel from the antenna bellow.

The Fig. 5 shows the evolution of the gain of the CTF (Channel Transfer Function) during the measurement. We can divide this figure in two parts :

1) From 0 to 13 s of measurement, it is the pNLOS part.
2) From 13s to the end of the measurement, it is the LOS part.

In the latter portion of the measurement, the presence of fading becomes evident. This fading indicates the existence of Multi-Path Components (MPCs). To further confirm this presence, the Power Delay Profile (PDP) of the two channels is plotted in Fig. 6 during the measurement. In this figure, we can observe not only the presence of fading, but also the existence of a multi-path component towards the end of the measurement. However, within this PDP, it is possible to identify the two aforementioned segments. The white line drawn on the Fig 6 represents the evolution of the main delay extracted from the GPS point from the RTK module. This line is correctly fitting the real evolution of the main path from the PDP, this is a good indication of the accuracy of the geolocation from the GPS RTK.

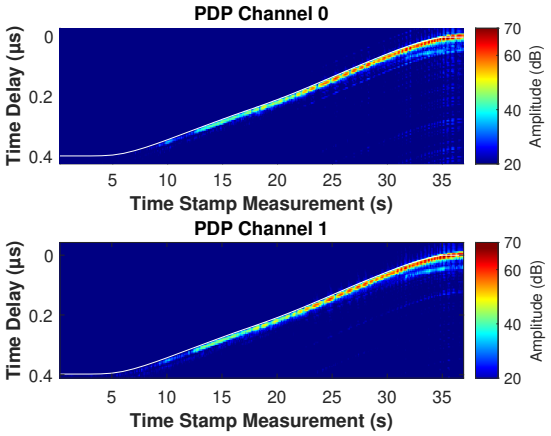

Fig. 6. The PDP for each channel. This plot shows the evolution of the PDP for all the measurement.

The limited bandwidth of the channel sounder prevents the identification of Multi-Path Components (MPCs) before the conclusion of the measurement. Nonetheless, the CTF gain from Fig. 5 indicates the presence of MPCs within the fading. To provide additional insight into the MPCs during the measurements, the Doppler function is plotted in Fig. 7. In the main line, we observe the presence of the Line Of Sight (LOS) component with information about the speed. This line approaches no Doppler as the measurement concludes when the car comes to a stop. Additionally, there are some lines descending from the main line to zero, indicating the existence of MPCs. The line in Fig. 7 at the 30-second mark originates from a parked vehicle near the road. In addition, the white line plot in the Fig 7 shows the estimated maximum doppler extracted from the velocity information included in the GNSS data. The small difference between the white line and the actual maximum doppler value indicated the accuracy of the speed information extracted from the GSP RTK data. An image of this environment is presented in Fig. 4.

In Fig. 5, the CTF gain can be fitted using a two-rays

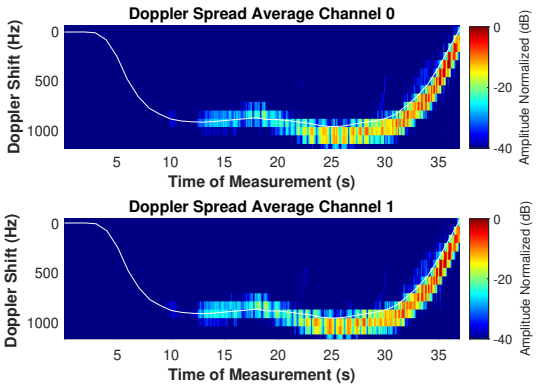

Fig. 7. The Doppler Spread Average function for all the measurement and each channel.

model. This model is characterized by a break point defined by equation 4, where $h1$ and $h2$ represent respectively the heights of Tx and Rx. In our specific configuration, $h1 = h2$, resulting in a break point at 6.4 km. Given our scenario with a maximum distance of 200 meters, we are significantly before the break point. Before this point, the model fits with a 20 dB slope, as shown in Fig. 5. In Fig. 8, we display the CTF gain for each channel and compare them to a two-rays channel model. The model aligns precisely with the measurements, as demonstrated by the proper fitting of the arches.

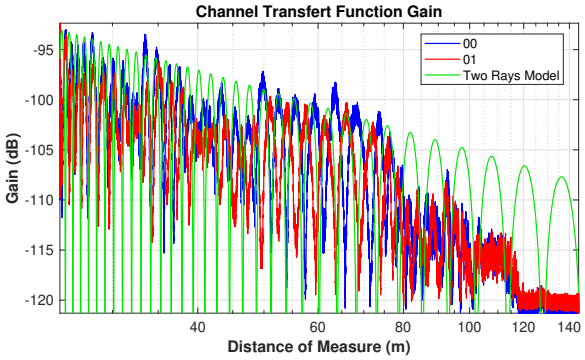

Fig. 8. The CTF gain for both channel (in blue and in red). The green curve represent a two rays channel model.

$$BP = \frac{4\pi h1 h2}{\lambda} \tag{4}$$

V. Conclusion

In this paper, we presented a radio channel characterization of a vehicle-to-infrastructure communication scenario, employing the IMT A's channel sounder with a center frequency of 60 GHz and the capability to conduct measurements for a couple of minutes. The objective is to establish a radio channel model based on the measurements for vehicle-to-infrastructure communication in sub-urban environment. In this specific scenario, a vehicle is used, with the transmitter (Tx) positioned on the car's roof, which travels from a distance of hundreds of meters.

A previous test campaign has been conducted to validate the channel sounder operation. This campaign validated the accuracy of the RTK GNSS module, the correct operation of all the upgrade imported on the CS including the fish eye camera.

The resulting measurements yield the gain of the Channel Transfer Function (CTF), which is then plotted and can be effectively fitted with a two-rays model. Additionally, the Power Delay Profile (PDP) is plotted, revealing the presence of Multi-Path Components (MPCs) towards the end of the measurement. Furthermore, the Doppler spread function is presented, illustrating the impact of vehicles parked around the track.

Acknowledgment

This work was performed under the mmW4Rail research project financed by the French Research Agency (ANR) under Grant ANR-20-CE22-0011.

References

[1] D. Dupleich, R. Muller, C. Schneider, S. Skoblikov, J. Luo, M. Boban, G. Del Galdo, and R. Thoma, "Multi-Band Vehicle to Vehicle Channel Measurements from 6 GHz to 60 GHz at "T" Intersection," in *2019 IEEE 2nd Connected and Automated Vehicles Symposium (CAVS)*. Honolulu, HI, USA: IEEE, Sep. 2019, pp. 1–5. [Online]. Available: https://ieeexplore.ieee.org/document/8887794/

[2] D. Dupleich, R. Müller, S. Skoblikov, C. Schneider, M. Boban, Jian Luo, G. Del Galdo, and R. Thomä, "Multi-band Spatio-Temporal Characterization of a V2V Environment Under Blockage," in *12th European Conference on Antennas and Propagation (EuCAP 2018)*. London, UK: Institution of Engineering and Technology, 2018, pp. 366 (5 pp.)–366 (5 pp.). [Online]. Available: https://digital-library.theiet.org/content/conferences/10.1049/cp.2018.0725

[3] A. Prokes, J. Blumenstein, J. Vychodil, T. Mikulasek, R. Marsalek, E. Zochmann, H. Groll, C. F. Mecklenbrauker, T. Zemen, A. Chandra, H. Hammoud, and A. F. Molisch, "Multipath Propagation Analysis for Vehicle-to-Infrastructure Communication at 60 GHz," in *2019 IEEE Vehicular Networking Conference (VNC)*. Los Angeles, CA, USA: IEEE, Dec. 2019, pp. 1–8. [Online]. Available: https://ieeexplore.ieee.org/document/9062771/

[4] J. Blumenstein, S. Sangodoyin, A. Molisch, A. Prokes, J. Vychodil, T. Mikulasek, E. Zochmann, H. Groll, C. F. Mecklenbrauker, M. Hofer, and T. Zemen, "Vehicle-to-Vehicle Millimeter-Wave Channel Measurements at 56-64 GHz," in *2019 IEEE 90th Vehicular Technology Conference (VTC2019-Fall)*. Honolulu, HI, USA: IEEE, Sep. 2019, pp. 1–5. [Online]. Available: https://ieeexplore.ieee.org/document/8891543/

[5] E. ZOchmann, M. Hofer, M. Lerch, J. Blumenstein, S. Sangodoyin, H. Groll, S. Pratschner, S. Caban, D. LOschenbr, L. BernadO, T. Zemen, A. Prokes, M. Rupp, C. F. Mecklenbrauker, and A. F. Molisch, "Statistical Evaluation of Delay and Doppler Spread in 60 GHz Vehicle-to-Vehicle Channels During Overtaking," in *2018 IEEE-APS Topical Conference on Antennas and Propagation in Wireless Communications (APWC)*. Cartagena des Indias: IEEE, Sep. 2018, pp. 1–4. [Online]. Available: https://ieeexplore.ieee.org/document/8503750/

[6] H. Groll, E. Zöchmann, S. Pratschner, M. Lerch, D. Schützenhöfer, M. Hofer, J. Blumenstein, S. Sangodoyin, T. Zemen, A. Prokes, A. F. Molisch, and S. Caban, "Sparsity in the Delay-Doppler Domain for Measured 60 GHz Vehicle-to-Infrastructure Communication Channels," Jan. 2019, arXiv:1901.10817 [eess]. [Online]. Available: http://arxiv.org/abs/1901.10817

[7] N. Attwood, M. Berbineau, F. Gallée, and P. Pajusco, "Experimental mmWave channel sounding in the 60 GHz band in railway environments," in *EuCap 23*, Apr. 2023.